Equal Channel Angular Pressing of a Newly Developed Precipitation Hardenable Scandium Containing Aluminum Alloy

Jahanzaib Malik, Wahaz Nasim, Bilal Mansoor, Ibrahim Karaman, Dinc Erdeniz, David C. Dunand, and David N. Seidman

Abstract

Precipitation hardenable aluminum alloys are well-known for their high strength-to-weight ratio, good thermal stability, electrical conductivity, and low cost. Equal channel angular pressing (ECAP) is proven to further improve the mechanical properties of metallic alloys through microstructure modification. In this work, ECAP of a recently developed, precipitation hardenable, cast Al–Er–Sc–Zr–V–Si alloy in peak-aged condition by route 4Bc was carried out to create an alloy with ultra-fine grain structure. The combined effect of grain refinement and precipitation on the tensile behavior and thermal stability of the ECAPed alloy is reported here. Improvement in yield strength and lack of strain hardening in ECAPed alloy were as expected. Microhardness contour plots with a narrower spread indicated enhancement in microstructural homogeneity after four ECAP passes as compared to the peak-aged condition. The variations in microhardness after annealing heat treatments at different temperatures highlighted the important role precipitates play in maintaining microstructure stability up to 250 °C in the ECAPed material.

Keywords

Aluminum alloy • Precipitation strengthening
ECAP • Microstructure

J. Malik · W. Nasim · B. Mansoor (✉) · I. Karaman
Department of Materials Science and Engineering, Texas A&M University, 575 Ross Street, College Station, TX 77843, USA

J. Malik
e-mail: jmalik@tamu.edu

B. Mansoor
Mechanical Engineering Program, Texas A&M University at Qatar, Education City, Doha, Qatar

D. Erdeniz · D. C. Dunand · D. N. Seidman
Department of Materials Science and Engineering, Northwestern University, 2220 Campus Drive, Evanston, IL 60208, USA

Introduction

Strengthening of materials at room temperature and elevated temperature is a comprehensive subject in materials science with a strong practical importance. The ultimate aim generally is to have materials with high strength-to-weight ratio, in order to achieve better efficiencies in high end applications. Precipitation hardening is one of the most effective strengthening processes which relies on alloying additions and heat-treatments to improve the mechanical response of metallic alloys [1]. Precipitation relies on solutes that have higher solubility at elevated temperatures and decreasing solubility at low temperatures [2].

Scandium containing aluminum alloys are readily used for high temperature applications due to their improved strength, toughness, creep resistance and good electrical properties [3]. The strengthening in these alloys is due to nano-sized and coherent tri-aluminide phases such as Al_3Sc. The mechanism of strengthening at ambient temperature is controlled by dislocation-precipitate interaction. Dislocations bypass the precipitates by shearing or Orowan looping mechanisms [4]. Continuous research in the optimization of the composition has allowed to develop aluminum alloys which can sustain temperatures as high as 400 °C. This has been made possible by the alloying additions of several rare-earth and transition metal elements that form $L1_2$ ordered trialuminide precipitates [5]. Additions of Zr, Er, and V has been reported to have a profound effect on the coarsening resistance of the precipitates due to their core/shell morphology [6–8]. Erdeniz et al. [9] has recently developed an aluminum alloy with micro-additions of Er, Sc, Zr, V, and Si. The authors reported a maximum hardness of ~600 MPa at ambient temperature after optimizing the peak-aging parameters. This is attributed to the precipitation strengthening due to the formation of $L1_2$-ordered Al_3(Sc,Er,Zr,V) nano-precipitates.

In addition to precipitation strengthening, severe plastic deformation (SPD) can be employed to further enhance

O. Martin (ed.), *Light Metals 2018*, The Minerals, Metals & Materials Series,
https://doi.org/10.1007/978-3-319-72284-9_57

strength through grain refinement in accordance with the Hall-Petch relationship [10–14]. Equal channel angular pressing (ECAP) is a popular SPD technique largely due to its strengthening effectiveness and processing efficiency [15–18]. Pre-ECAP aging and post-ECAP aging are the two main processing sequences that are used to optimize the strengthening of precipitation hardenable alloys. In the post-ECAP aging category, many authors have investigated the effect of ECAP on precipitation kinetics and the link between high density of lattice defects and diffusion controlled processes [19–21]. In the pre-ECAP aging, major areas of concern are the influences of deformation during ECAP on the precipitates distribution [22], fracturing [23], coarsening/dissolution [24], and subsequent microstructure stability at elevated temperatures.

In this study, a newly developed precipitation hardened Al–Sc–V–Er–Zr–Si alloy by Erdeniz et al. [9], in peak aged condition was subjected to equal channel angular pressing using route 4Bc. It is to be noted that only the effects of ECAP on aged alloy has been reported here. ECAP of the homogenized alloy is another extensive study and will be reported elsewhere. The effect of ECAP on the grain refinement and subsequent improvement in mechanical properties were studied using tensile tests and microhardness contour maps. In addition, thermal stability of ECAPed microstructure was evaluated by taking microhardness measurements after conducting annealing heat treatments at various temperatures. Lastly, scanning electron microscopy (SEM) was used to evaluate the influence of ECAP on precipitate distribution, coarsening/dissolution, and fracturing, if any.

Experimental Procedure

Alloy Production and Aging Heat Treatments

The alloy used in this study is cast aluminum with micro-alloying additions of Sc, Er, Zr, V, and Si. Nominal composition of Al–Sc–Er–Zr–V–Si is given in Table 1. The detailed casting procedure for this alloy has been reported in the previous study [9]. Three as-cast billets were solution-treated at 640 °C for 4 h. One of the billets was kept in the homogenized (H) state for reference. The other two billets were aged using a two-step aging treatment of 350 °C/16 h followed by 400 °C/12 h. The effectiveness of this double aging treatment has been previously reported by Erdeniz et al. [9]. All heat-treated billets were quenched in water to terminate the treatment.

ECAP Processing

One of the two aged billets was subjected to ECAP at room temperature, with a pressing speed of 1 mm/min, using a 90° die channel. This billet will be referred as PA-ECAP. Aluminum foil wrapping was used to reduce the friction between the billet and the die. The schematic of ECAP process is shown in Fig. 1. Three directions (extrusion, normal and flow direction) and their corresponding orthogonal planes are also given in the figure. Only flow plane was used for microstructure characterization and microhardness measurements. Route Bc with four passes was utilized in this study, which corresponds to the rotation of billet by 90° after each pass. This particular route was selected based on its established efficacy in obtaining uniform ultra-fine grain structure with high angle of misorientation as reported by several researchers for a range of different metallic alloys including aluminum [14, 25, 26]. Furthermore, four and more passes can accumulate sufficient strains to induce high-angle grain boundaries [27].

Mechanical Characterization

Room temperature tensile tests and Vickers microhardness measurements were carried out on three specified conditions: (1) Homogenized only (H), (2) Peak-aged (PA), and (3) Peak-aged followed by ECAP (PA-ECAP). Tensile tests were conducted at a constant strain rate of 1×10^{-3} s^{-1} using an electromechanical MTS Insight 30 kN machine. Schematic of the miniature tensile specimen used in this study is given in Fig. 2. Two specimens were tested at this condition to ensure repeatability.

To study the hardness distribution and homogeneity, microhardness measurements on above-mentioned three conditions were carried out using 50 gf load and an indentation time of 10 s. Specimens of size 1 × 1 cm size were cut and polished down to 1 µm diamond polish to obtain a mirror-like finish. A grid profile was made with 1 mm step size in both x and y directions and then represented using contour plots.

Microhardness measurements after annealing heat treatments on PA and PA-ECAP specimens were taken to

Table 1 Composition in at. %, of alloying additions in aluminum

Sc	Er	Zr	V	Si	Al
0.013	0.007	0.071	0.074	0.054	Bal.

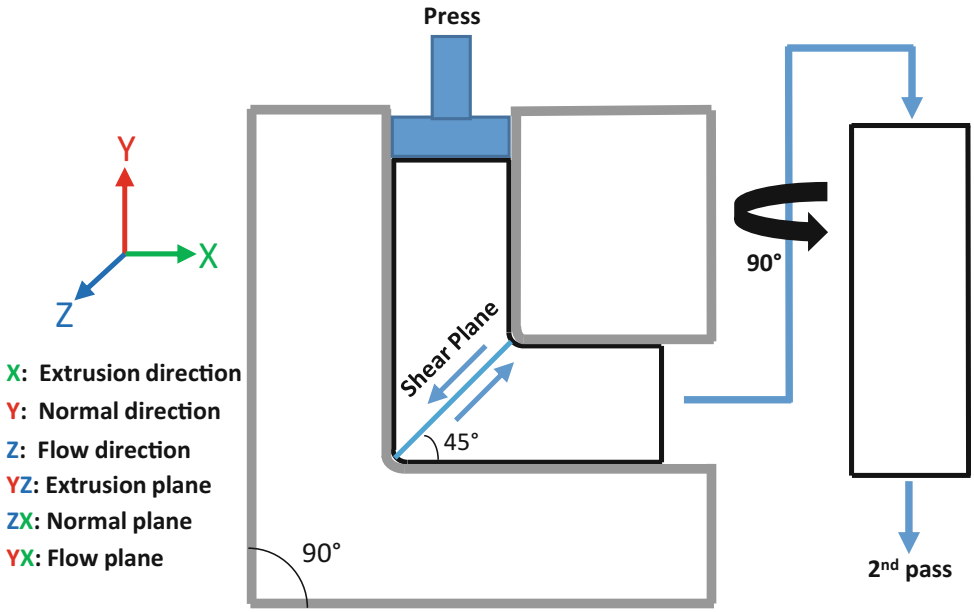

Fig. 1 Schematic of an ECAP process illustrating orthogonal directions and planes. For route Bc, the billet was rotated 90° along y-axis, after each such pass as shown in the figure

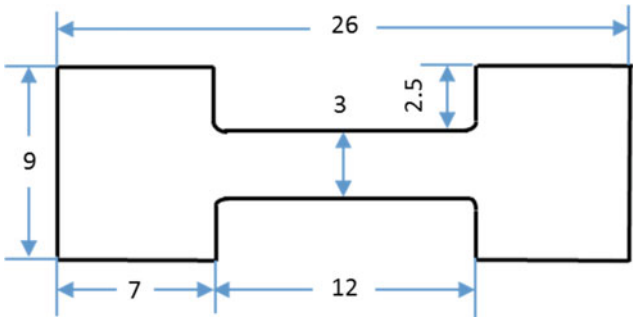

Fig. 2 Sketch with dimensions of a miniature specimen used for tensile testing. All dimensions are in millimeters

evaluate the thermal stability and grain coarsening resistance at elevated temperatures. Annealing heat treatments were carried out using the temperature range from 50 to 550 °C with 50 °C increments and holding time of 3 h at each temperature. In some limited cases, annealing data from an ECAPed (route 4Bc), commercially pure aluminum alloy (Al-1100) was included as a reference.

Microstructure Characterization

All specimens for microstructure characterization were cut from the center of the cast billet and the flow plane of the ECAPed billet, using electro discharge machining. Specimens were ground down to 1200 grit size, followed by polishing using 3 and 1 µm diamond paste and 0.04 µm colloidal silica. Optical microscopy was employed to measure the grain sizes of H and PA specimens. Specimens were etched using Keller's reagent (20 mL HNO_3, 20 mL HCl, 5 mL and 20 mL H_2O) and observed under the light microscope to reveal the grain boundaries.

EBSD analysis was performed to observe the microstructural changes and obtain a map of grain size and orientation after ECAP. A FERA SEM with an EBSD attachment was used for mapping. The PA-ECAP specimen of area 25 × 25 µm was scanned using at a step size of 0.1 µm. Map noise reductions was conducted to the fifth degree before grain size and misorientation measurements. In addition, a FEI Quanta 400 SEM was employed to study the distribution of precipitates in the annealed PA-ECAP specimens and to explain their role in maintaining thermal stability. Imaging was done using a backscattered electron detector and an accelerating voltage of 20.0 kV.

Results and Discussion

The comparison of grain sizes in the optical images of H and PA, and EBSD map of PA-ECAP specimens are shown in Fig. 3. Average grain size of H is 411 ± 232 µm and of PA is slightly coarser, 656 ± 385 µm. Larger grain size in PA was caused by the two-step aging treatment after homogenized condition. Another observation on H and PA micrographs is the subgrain structure seen (approximately 40 µm) in some of the grains, which may have been caused by the remnant primary precipitates that formed during solidification. These precipitates may inhibit recrystallization during the homogenization and aging treatments, as stated in previous studies [28, 29]. EBSD maps of the flow plane of PA-ECAP is shown in Fig. 3c. Color mapping orientation was with respect to the Z direction for each sample (out of

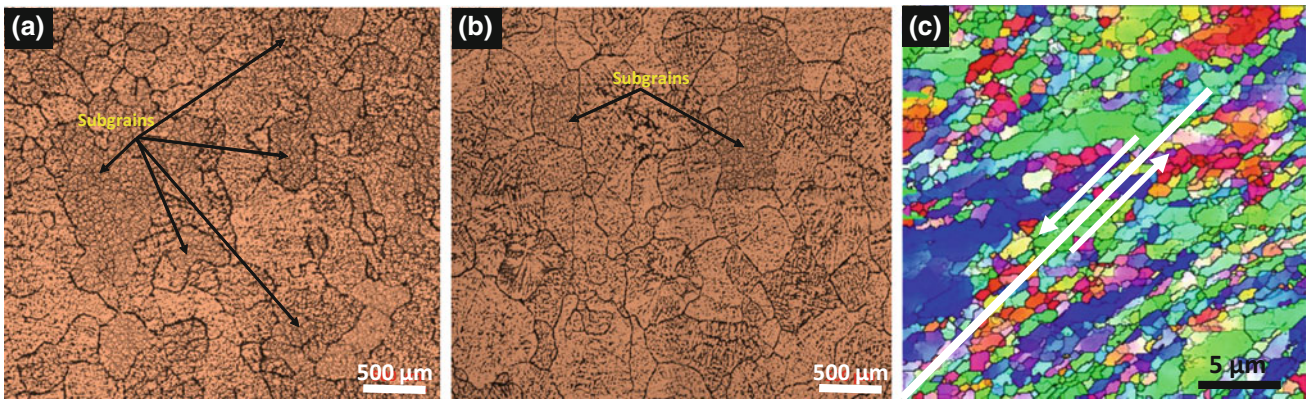

Fig. 3 Optical micrographs of **a** Homogenized (H) and **b** Peak-aged (PA) specimens, at a magnification of 5X. EBSD map of **c** PA-ECAP (flow plane) specimen, showing grains oriented along the shear plane. Theoretical shear plane at 45° is shown by white line in (**c**)

the page). Ultrafine grain size of 0.78 ± 0.44 µm was obtained after ECAP. Grains and sub grains can be clearly seen oriented and elongated along the shear plane.

Room temperature stress vs. strain plots obtained at a constant strain rate of 1×10^{-3} s^{-1}, are shown in Fig. 4. The relevant values of tensile data are given in Table 2. Three cases of strengthening can be seen here: (1) Solute strengthening (H), where most of the alloying elements are present in the form of a solid solution. The strength is low and mainly due to the interaction of dislocation with solute atoms, but large ductility of 31.6% is obtained. (2) Precipitation strengthening (PA), where most of the solute atoms have precipitated out after aging treatments, in the form of tri-aluminide precipitates. These precipitates are elastically hard, coarsening resistant and coherent in nature, and exhibit high strength due to elastic interactions exerted by the mismatch in lattice parameter and precipitate-matrix modulus [30]. As a result, we see a 2.3 times increase in yield strength as compared to the homogenized (H) condition, along with noticeable work hardening, and 6% decrease in ductility. (3) Combination strengthening (PA-ECAP), where major source of strength is due to grain refinement, in accordance with Hall-Petch relationship, and some contribution is possibly due to the precipitate hardening. Consequently, maximum yield strength of 178.3 MPa was obtained at the expense of ductility. The decrease in ductility with increasing strength is due to insufficient strain hardening, as explained by Wang and Ma [31].

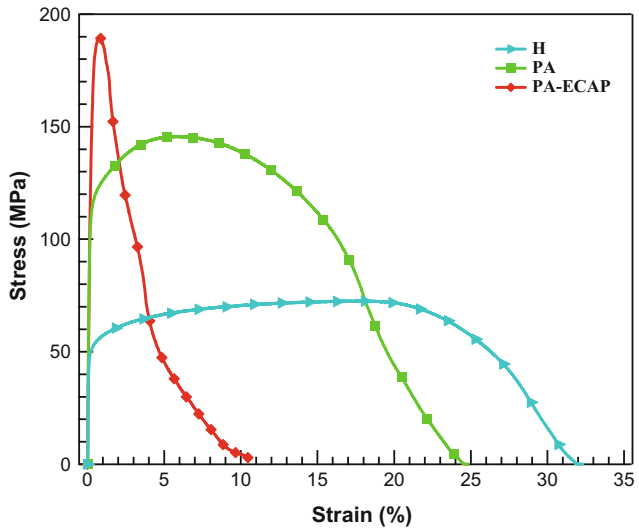

Fig. 4 Tensile tests at a constant strain rate of 10^{-3} s^{-1} for three different processing conditions. A general trend of high yield stress and low ductility is observed after successive strengthening processes

Figure 5 shows the contour plots of microhardness of the three conditions. This was done to illustrate the microhardness homogeneity after aging and ECAP. A very small microhardness spread of 27–30 HV in H shows that the primary precipitates which may have formed during solidification and remained undissolved during the homogenization treatment, have negligible effect on localized or overall strengthening. For PA specimen, the microhardness distribution across the cross-section ranging from 48 to 55 HV, indicates slight inhomogeneity with high values at some local points, highlighted in orange color on the contour map. After ECAP there is homogeneity in the microstructure with microhardness distribution in the range of 59–63 HV. This is mainly attributed to the uniform grain refinement after ECAP. Xu and Langdon [32] studied the hardness homogeneity after ECAP in aluminum and its alloy and concluded that it gradually increases with number of passes.

Figure 6 shows the annealing heat treatment curves for PA, PA-ECAP and Al-1100-ECAP. Pure aluminum alloy shows a sudden drop in microhardness after annealing at 150 °C for 3 h, followed by a sharp drop to 30 HV after 250 °C for 3 h, and ultimately reaching the nominal microhardness of 25 HV after 400 °C/3 h. This trend is

Table 2 Summary of the results from tensile tests, microhardness measurements and microstructure analysis

Designation	Yield strength at 10^{-3} s^{-1} strain rate (MPa)	Elongation at 10^{-3} s^{-1} strain rate (%)	Mean microhardness (HV)	Average grain size (μm)
H	50.7	31.6	29.4	411 ± 232
PA	115.6	24.2	52.4	656 ± 385
PA-ECAP	178.3	10.4	62.3	0.78 ± 0.44

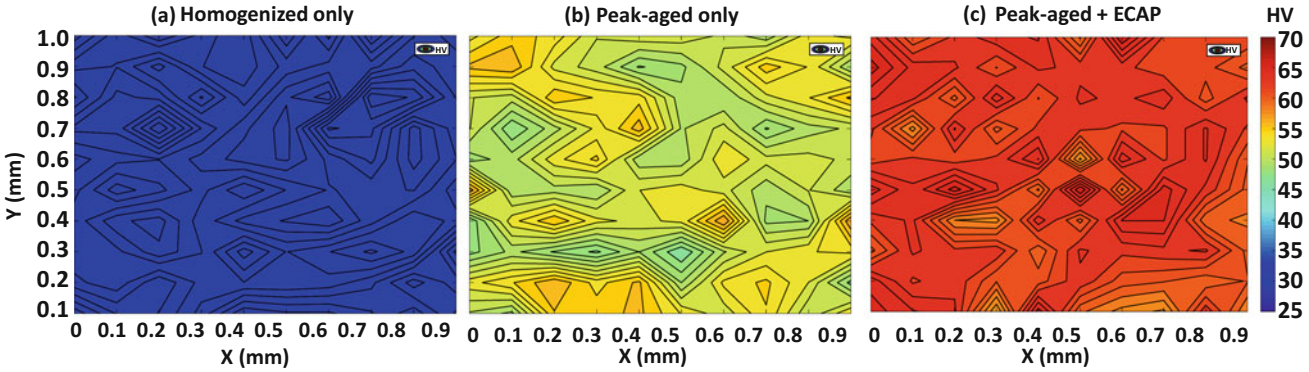

Fig. 5 Contour plots showing Vickers microhardness distribution in 1 × 1 cm cross-section of **a** H, **b** PA, and **c** PA-ECAP

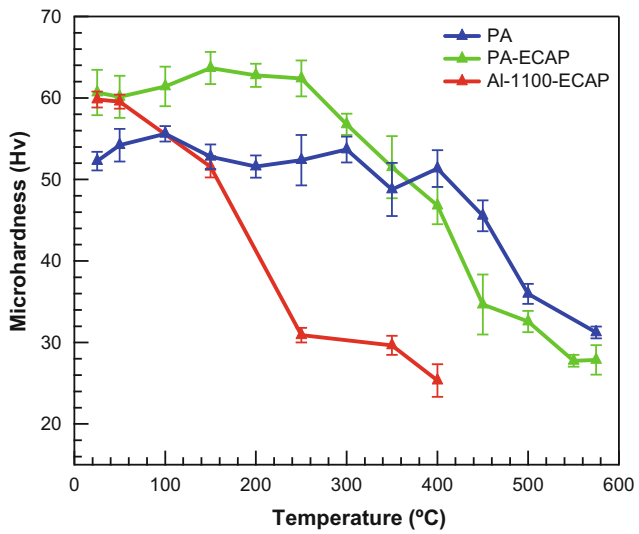

Fig. 6 Microhardness measurements after annealing heat treatments on PA-ECAP and Al-1100-ECAP. Commercially pure Al-1100 was also ECAPed using route 4Bc and used here as a reference

quite expected and is mainly due to rapid recrystallization and grain growth during annealing. Contrasting trend of microhardness can be seen in the newly developed alloy in PA and PA-ECAP conditions. PA shows slight increase up to 100 °C, thereafter displays a fairly small decrease in microhardness up until 400 °C. Sharp drops in microhardness beyond 400 °C corresponds to coarsening and dissolution of precipitates [9]. Nevertheless, annealing trend of PA indicates the potential of precipitates in maintaining the strength of the alloy when exposed to elevated temperatures. PA-ECAP alloy has fine grain structure and homogenous distribution of precipitates after ECAP, as illustrated by EBSD map and microhardness contour plots. Annealing heat treatments on PA-ECAP shows a slight increase in microhardness at 150 °C and thermal stability up until 250 °C. The main difference between PA-ECAP and Al-1100 is of course the presence of finely distributed, nanosized, coarsening resistant tri-aluminide precipitates. Thus, it is evident that when exposed to elevated temperatures these precipitates play a role of inhibiting, restraining and delaying the grain growth, therefore maintaining the combined strengthening [29]. Microhardness eventually drops at temperatures greater than 300 °C, this is due to concurrent recrystallization, grain growth, and to a lesser extent, precipitate coarsening at elevated temperatures.

Size and distribution of precipitates after annealing at given temperatures is shown in Fig. 7. All the SEM images are captured from the flow plane of the ECAPed billet. The arrangement of precipitates follows a definite trend and are distributed along the shear plane, which is at ∼45° angle from the longitudinal plane as illustrated in Fig. 7a. Elongated grains in the same direction are also visible (Fig. 7d). The precipitates can also be seen decorating along the grain boundaries, more prominently in Fig. 7e, f. These precipitates play a significant role in restraining the grain growth during annealing, thus maintaining the thermal stability of the microstructure. Precipitates sizes in these alloys are in

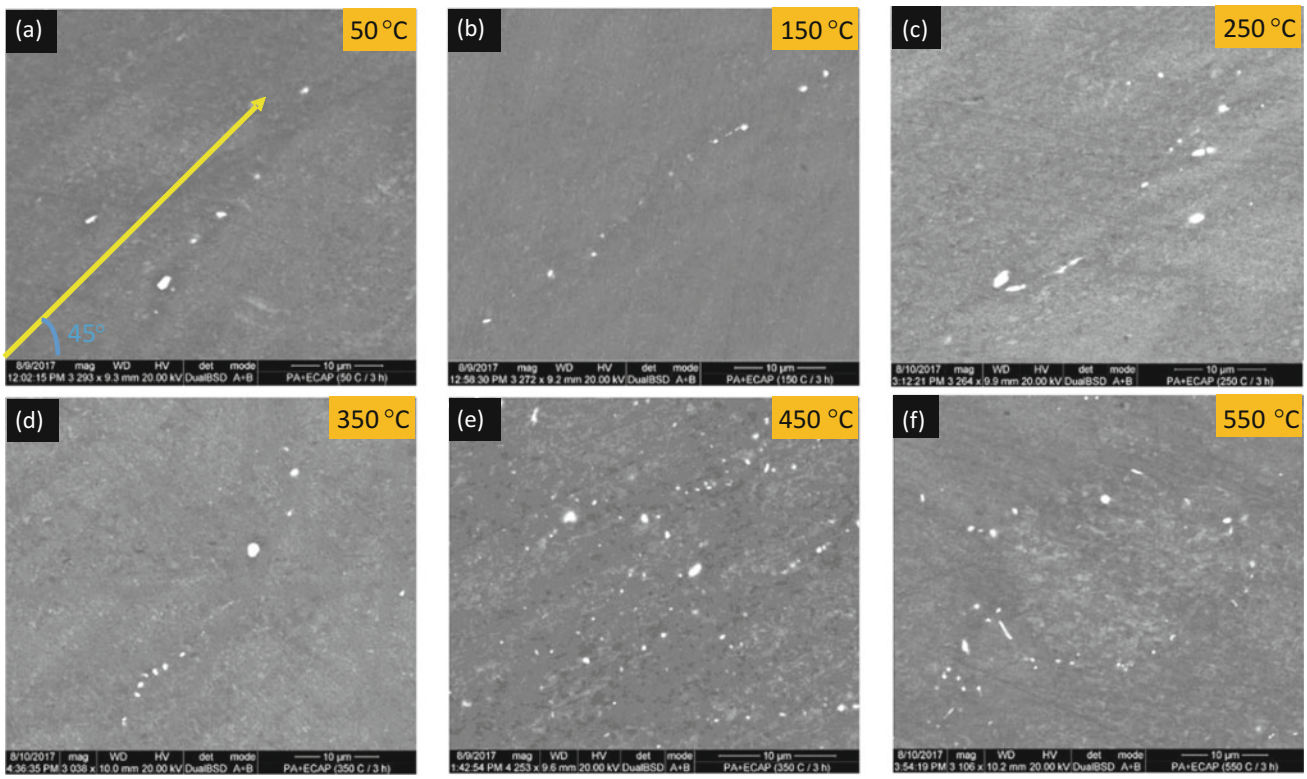

Fig. 7 Scanning electron microscopy images after various step of annealing heat treatment. At each temperature, the specimen was held for 3 h and then quenched in water

the range of 50–500 nm, although sizes observed in previous studies are in the range of 10–100 nm [3, 8, 33]. Due to the fine scale of precipitates, the true number density of precipitates cannot be resolved in Fig. 7a–d. These precipitates become visible at higher temperatures (Fig. 7e–f) as a result of coarsening. Though, no evidence of fracturing or dissolution was observed in any case. In-depth TEM analysis may be required to have a better estimation of the precipitate number density. In addition to TEM analysis, it would be interesting to research how the precipitates evolve during ECAP and post-ECAP aging of a homogenized Al–Sc–V–Er–Zr–Si alloy. We expect a significant increase in precipitation kinetics after ECAP of a supersaturated alloy. This is currently the focus of another ongoing study.

Conclusions

The effect of ECAP on the grain refinement and subsequent improvement in mechanical properties of Al–Sc–V–Er–Zr–Si alloy was studied using tensile tests, microhardness contours, heat treatments and microscopic imaging. Following conclusion can be drawn from this study:

1. Grain size refinement from 656 ± 385 µm to 0.78 ± 0.44 µm resulted after ECAP. Extensive sub-grain formation was observed. Grains were oriented along the shear plane.
2. Enhancements in mechanical properties after ECAP was as expected, with a ~55% increase in yield strength from peak-aged condition. This was attributed to the combined strengthening due to grain refinement and precipitate hardening. However, insufficient strain hardening capability resulted in the reduction of ductility.
3. Homogenous microstructure and distribution of precipitates after ECAP of peak-aged specimen resulted in hardness homogeneity across the specimen.
4. Annealing heat treatments show that precipitates play a vital role in maintaining microhardness by inhibiting and restraining grain growth at elevated temperatures. Therefore, the ECAPed alloy maintains thermal stability up to 250 °C/3 h.

Acknowledgements This work was made possible by a National Priorities Research Program grant from the Qatar National Research Fund (a member of The Qatar Foundation), under grant number NPRP 7-756-2-284. The statements made herein are solely the responsibility of the authors.

References

1. I. J. Polmear (1996) Recent Developments in Light Alloys. Mater. Trans. JIM, 37(1):12–31.
2. G. E. Dieter and D. Bacon (1962) Mechanical metallurgy. Journal of the Franklin Institute, 273(4):338.
3. D. N. Seidman, E. A. Marquis, and D. C. Dunand (2002) Precipitation strengthening at ambient and elevated temperatures of heat-treatable Al(Sc) alloys. Acta Mater., 50(16):4021–4035.
4. K. E. Knipling, D. N. Seidman, and D. C. Dunand (2011) Ambient- and high-temperature mechanical properties of isochronally aged Al-0.06Sc, Al-0.06Zr and Al-0.06Sc-0.06Zr (at.%) alloys. Acta Mater., 59(3):943–954.
5. R. A. Karnesky, M. E. van Dalen, D. C. Dunand, and D. N. Seidman (2006) Effects of substituting rare-earth elements for scandium in a precipitation-strengthened Al-0.08 at. %Sc alloy. Scr. Mater., 55(5):437–440.
6. C. Booth-Morrison, D. N. Seidman, and D. C. Dunand (2012) Effect of Er additions on ambient and high-temperature strength of precipitation-strengthened Al-Zr-Sc-Si alloys. Acta Mater., 60 (8):3643–3654.
7. A. De Luca, D. C. Dunand, and D. N. Seidman (2016) Mechanical properties and optimization of the aging of a dilute Al-Sc-Er-Zr-Si alloy with a high Zr/Sc ratio. Acta Mater., 119:35–42.
8. M. E. Van Dalen, T. Gyger, D. C. Dunand, and D. N. Seidman (2011) Effects of Yb and Zr microalloying additions on the microstructure and mechanical properties of dilute Al-Sc alloys. Acta Mater., 59(20):7615–7626.
9. D. Erdeniz, W. Nasim, J. Malik, A. R. Yost, S. Park, A. De Luca, N. Q. Vo, I. Karaman, B. Mansoor, D. N. Seidman, and D. C. Dunand (2017) Effect of vanadium micro-alloying on the microstructural evolution and creep behavior of Al-Er-Sc-Zr-Si alloys. Acta Mater., 124:501–51.
10. E. O. Hall (1951) The Deformation and Ageing of Mild Steel: III Discussion of Results. Proc. Phys. Soc. Sect. B, 64(9):747.
11. N. J. Petch (1953) The cleavage strength of polycrystals. J. Iron Steel Inst. Lond., 173:25–28.
12. A. Dubyna, A. Mogucheva, and R. Kaibyshev (2014) Hall-Petch Relationship in an Al-Mg-Sc Alloy Subjected to ECAP. Adv. Mater. Res., 922:120–125.
13. M. Furukawa, Z. Horita, M. Nemoto, R. Z. Valiev, and T. G. Langdon (1996) Microhardness measurements and the hall-petch relationship in an Al-Mg alloy with submicrometer grain size. Acta Mater., 44(11):4619–4629.
14. Y. Iwahashi, M. Furukawa, Z. Horita, M. Nemoto, and T. G. Langdon (1998) Microstructural characteristics of ultrafine-grained aluminum produced using equal-channel angular pressing. Metall. Mater. Trans. A, 29(9):2245–2252.
15. V. M. Segal, V. I. Reznikov, A. E. Dobryshevshiy, and V. I. Kopylov (1981) Plastic working of metals by simple shear. Russ. Metall., 1:99–105.
16. V. M. Segal (1995) Materials processing by simple shear. Mater. Sci. Eng. A, 197(2):157–164.
17. Z. Horita, T. Fujinami, M. Nemoto, and T. G. Langdon (2001) Improvement of mechanical properties for Al alloys using equal-channel angular pressing. J. Mater. Process. Technol., 117(3):288–292.
18. M. Furukawa, Y. Iwahashi, Z. Horita, M. Nemoto, and T. G. Langdon (1998) The shearing characteristics associated with equal-channel angular pressing. Mater. Sci. Eng. A, 257(2): 328–332.
19. M. Fujda, M. Matvija, T. Kvačkaj, O. Milkovič, P. Zubko, and K. Nagyová (2012) Structure and properties of AlMgSi alloys after ECAP and post-ECAP ageing. Mater. Tehnol., 46(5):465–469.
20. W. J. Kim and J. Y. Wang (2007) Microstructure of the post-ECAP aging processed 6061 Al alloys. 464:23–27.
21. S. Farè, N. Lecis, and M. Vedani (2011) Aging Behaviour of Al-Mg-Si Alloys Subjected to Severe Plastic Deformation by ECAP and Cold Asymmetric Rolling. J. Metall. 2011:1–8.
22. C. Xu, M. Furukawa, Z. Horita, and T. G. Langdon (2005) Influence of ECAP on precipitate distributions in a spray-cast aluminum alloy. Acta Mater., 53(3):749–758.
23. V. L. Sordi, C. A. Feliciano, and M. Ferrante (2015) The influence of deformation by equal-channel angular pressing on the ageing response and precipitate fracturing: case of the Al–Ag alloy. J. Mater. Sci., 50(1):138–143.
24. J. Gubicza, I. Schiller, N. Q. Chinh, J. Illy, Z. Horita, and T. G. Langdon (2007) The effect of severe plastic deformation on precipitation in supersaturated Al-Zn-Mg alloys. Mater. Sci. Eng. A, 460–461:77–85.
25. T. G. Langdon (2007) The principles of grain refinement in equal-channel angular pressing. Mater. Sci. Eng. A, 462(1):3–11.
26. R. E. Barber, T. Dudo, P. B. Yasskin, and K. T. Hartwig (2004) Product yield for ECAE processing. Scr. Mater., 51(5):373–377.
27. Y. Estrin, M. Murashkin, and R. Valiev (2010) Ultrafine grained aluminium alloys: processes, structural features and properties. Fundamentals of Aluminium Metallurgy: Production, Processing and Applications, Woodhead Publishing Limited, Cambridge 468–503.
28. V. S. Zolotorevsky, N. A. Belov, and M. V Glazoff (2007) Casting aluminum alloys 12. Elsevier Amsterdam.
29. A. Association (1984), Aluminum: properties and physical metallurgy. ASM International.
30. K. E. Knipling, D. C. Dunand, and D. N. Seidman (2006) Criteria for developing castable, creep-resistant aluminum-based alloys – A review. Zeitschrift für Met., 97(3):246–265.
31. Y. M. Wang and E. Ma (2004) Strain hardening, strain rate sensitivity, and ductility of nanostructured metals. Mater. Sci. Eng. A, 375–377(1–2):46–52.
32. C. Xu and T. G. Langdon (2007) The development of hardness homogeneity in aluminum and an aluminum alloy processed by ECAP. J. Mater. Sci., 42(5):1542–1550.
33. E. A. Marquis and D. N. Seidman (2001) Nanoscale structural evolution of Al_3Sc precipitates in Al(Sc) alloys. Acta Mater., 49(11):1909–1919.